Two-Dimensional (2+*n*) REMPI of CH_3Br: Photodissociation Channels via Rydberg States

Ágúst Kvaran,* Huasheng Wang, and Kristján Matthíasson

Science Institute, University of Iceland, Dunhagi 3, 107 Reykjavík, Iceland

Andras Bodi

Molecular Dynamics Group, Paul Scherrer Institut, 5232 Villigen, Switzerland

Received: May 6, 2010; Revised Manuscript Received: August 3, 2010

(2+*n*) resonance enhanced multiphoton ionization (REMPI) spectra of CH_3Br for the masses H^+, CH_m^+, $^iBr^+$, H^iBr^+, and $CH_m{}^iBr^+$ ($m = 0-3$; $i = 79, 81$) have been recorded in the 66 000−81 000 cm^{-1} resonance energy range. Signals due to resonance transitions from the zero vibrational energy level of the ground state CH_3Br to a number of Rydberg states $[\Omega_c]nl;\omega$ ($\Omega_c = 3/2, 1/2$; $\omega = 0, 2$; $l = 1$(p), 2(d)) and various vibrational states were identified. $C(^3P)$ and $C^*(^1D)$ atom and HBr intermediate production, detected by (2+1) REMPI, most probably is due to photodissociation of CH_3Br via two-photon excitations to Rydberg states followed by an unusual breaking of four bonds and formation of two bonds to give the fragments H_2 + C/C* + HBr prior to ionization. This observation is supported by REMPI observations as well as potential energy surface (PES) ab initio calculations. Bromine atom production by photodissociation channels via two-photon excitation to Rydberg states is identified by detecting bromine atom (2+1) REMPI.

Introduction

Spectroscopy[1–6] and photofragmentation[7–13] of methyl bromide has received considerable interest over the last decades, both experimentally[1–12] and theoretically,[13] for a number of reasons. Methyl bromide as well as the chlorine and iodine containing methyl halides play important roles both in the chemistry of the atmosphere[6,14–16] and in industry. Thus, although far less abundant than methyl chloride in the stratosphere, methyl bromide is found to be much more efficient in ozone depletion[16] and is now being phased out under the Montreal Protocol. Furthermore, bromocarbons are known to have a high global warming potential.[17] Additionally, the molecule is a simple prototype system of a halogen containing organic molecule for fundamental studies of photodissociation and photoionization processes.[10,13,18]

Little is known about the UV spectroscopy of methyl bromide despite its importance in various contexts. Since a pioneering work by Price[1] in 1936 some absorption studies have appeared dealing with (i) a weak continuous spectrum (the A band) in the low energy region ($\lambda > 180$ nm; $\bar{E} < 55\,500$ cm^{-1})[2,6,14,15] due to transitions to repulsive states[13] and (ii) higher energy ($\lambda < 180$ nm; $\bar{E} > 55\,500$ cm^{-1}) Rydberg series and its vibrational analysis.[2–5] There has been some controversy in the literature concerning the assignment of the higher energy band spectra. Locht et al. recently reported analysis and assignments of spectra[4,5] that differ from earlier reports.[1–3] More recently, however, multiphoton absorption (REMPI) studies[18] and ab initio calculations of excited states[19] have been published that help clarify the discrepancy.

Photofragmentation studies of methyl bromide can be classified into two groups. One group focuses on the characterization of photofragments CH_3 + $Br(^2P_{3/2})$/$Br^*(^2P_{1/2})$ resulting from photodissociation in the A band[7–10,13] whereas the other group concerns the $CH_3^+ + Br^-$ ion-pair formation[11,12,18] in the energy region between the ion-pair formation threshold (76 695 cm^{-1}) and the ionization energy (85 031.2 cm^{-1} for $CH_3Br^+(^2\Pi_{3/2})$; 87 615.2 cm^{-1} for $CH_3Br^+(^2\Pi_{1/2})$).[18] To our knowledge no other photofragmentation channels have been reported so far. Some disagreement concerning the ion-pair formation is to be found in the literature. Thus Xu et al.[12] and Shaw et al.[11] conclude that direct excitation to the ion-pair state is the major step prior to ion-pair formation whereas more recently Ridley et al.[18] give evidence for Rydberg doorway states in the photoion pair formation analogous to observations for some halogen containing diatomic molecules.[20–24]

The basic picture for the electron configuration of the methyl halides is analogous to that for the hydrogen halides, such that, in the first approximation, the symmetry notation C_{3v}, which holds for the methyl halides, can be replaced by $C_{\infty v}$.[19] Excited state potentials for the methyl halides (CH_3X; X = Cl, Br, I) as a function of the C−X bond closely resemble those for the HX molecules showing (i) a number of repulsive valence state potentials that correlate with the CH_3 + $Br(^2P_{3/2})$/$Br^*(^2P_{1/2})$ species, (ii) a series of Rydberg state potentials that closely resemble the neutral and first ionic ground state potentials, and (iii) an ion-pair $^1A_1(C_{3v})$ ($^1\Sigma(C_{\infty v})$) state with large average internuclear distance. Characteristic state interactions between Rydberg and the ion-pair states are found to affect the spectroscopy and excited state dynamics for the hydrogen halides.[25–34] It has been pointed out that analogous effects are to be found for methyl bromide.[18,19]

In this paper we report a two-dimensional (2+*n*) REMPI experiment analogous to those presented before for acetylene[35] and HCl,[25,34,36] which helps elucidate the discrepancy concerning the VUV spectroscopy of methyl bromide, and which also yields evidence for new photodissociation channels via Rydberg states. First, it allows us to assign several new vibronic bands and to confirm the assignment by Causley and Russel based on single photon absorption data.[2] Second, C atom and HBr molecule REMPI signals in the 2D REMPI data show that CH_3Br Rydberg

* Author for correspondence. Phone: +354-525-4694 (A.K.'s office), +354-525-4800 (main office). Fax: +354-552-8911 (main office). E-mail: agust@hi.is. Homepage: http://www.hi.is/~agust/.

10.1021/jp104128j
Published on Web 08/20/2010

states may photodissociate to form $H_2 + C(^3P)/C^*(^1D) + HBr$. Third, strong bromine atom REMPI signals following two-photon excitation to Rydberg states as well as power dependence analysis of the signals is indicative of important predissociation channels leading to $Br(^2P_{3/2})$ and $Br^*(^2P_{1/2})$.

Experimental Section

The apparatus used has been described elsewhere, and only a brief overview is given here.[25,34–36] Mass spectra for masses 1 amu (H^+) to 96 amu ($CH_3{}^{81}Br^+$) were recorded for the two-photon excitation region 66 000−81 500 cm^{-1} (one-photon wavelength region 245−303 nm. Tunable excitation radiation was generated by Excimer laser-pumped dye laser systems, using a Lambda Physik COMPex 205 Excimer laser and a Coherent ScanMatePro dye laser at a typical repetition rate of 10 Hz. Dyes R610, R590, R540A, and C503 were used and frequency doubling performed with KDP and BBO-2 crystals. The bandwidth of the dye laser beam was about 0.095 cm^{-1}. The typical laser intensity used was 0.1−0.3 mJ/pulse. Undiluted, pure CH_3Br gas sample (Merck Schuchardt; purity 99.5%) was used. It was pumped through a 500 μm pulsed nozzle from a typical total backing pressure of about 1.0−1.5 bar into an ionization chamber. The pressure in the ionization chamber was lower than 10^{-6} mbar during experiments. The nozzle was kept open for about 200 μs, and the laser beam was typically fired 500 μs after the nozzle was opened. Ions were extracted into a time-of-flight tube and directed on an MCP detector, whose signal was fed into a LeCroy 9310A, 400 MHz storage oscilloscope, to record the time-of-flight distributions. The average signal levels were evaluated and recorded for a fixed number of laser pulses (typically 100 pulses) to obtain the mass spectra. Mass spectra were typically recorded in 0.1 or 0.2 cm^{-1} laser wavenumber steps to obtain 2D REMPI spectra. REMPI spectra for certain ions as a function of excitation wavenumber (1D REMPI) were obtained by integrating signal intensities for the time-of-flight ranges corresponding to the particular ion mass. The power dependence of the ion signal was determined by averaging for ca. 1000 pulses, after bypassing a different number of quartz windows to reduce power. Care was taken to prevent saturation effects as well as power broadening by minimizing laser power. Laser calibration was performed by recording an optogalvanic spectrum, obtained from a built-in neon cell, simultaneously with the recording of the REMPI spectra. The accuracy of the calibration was found to be about ± 2.0 cm^{-1} on a two-photon wavenumber scale. Intensities were corrected for laser power and drifts during the scans. Overall spectra are composed of several shorter scans, each of which were normalized to the square of the laser intensity, which corresponds to a power dependence of (2+1)REMPI under steady-state conditions. These scans are then normalized to each other using the intensities of bands that are common to neighboring sections. However, some uncertainties in the relative intensities of the bands remain.

Results and Analysis

Mass and REMPI Spectra. Figure 1a shows a typical mass spectrum recorded at the 66 022 cm^{-1} two-photon laser excitation corresponding to the [3/2]5p;0 Rydberg state, zero vibrational energy band ($v_i' = 0$ for all vibrational modes i).[18] Ions observed are H^+, $CH_m{}^+$ ($m = 0-3$), ${}^iBr^+$ ($i = 79, 81$), and $CH_m{}^iBr^+$ ($m = 0-3$; $i = 79, 81$). Except for C and Br atom resonance wavelengths (see below) the strongest signal is observed for $CH_3{}^+$. Mass signals for the $CH_m{}^+$ ($m = 0-3$) ions vary in intensity as $CH_3{}^+ > CH_2{}^+ > CH^+ > C^+$. Mass signals for ${}^iBr^+$, $CH_m{}^iBr^+$, and H^+ are very weak compared to those for $CH_3{}^+$. Typically, C^iBr^+ ($i = 79$ and 81) ion signals are found to be the strongest among the $CH_m{}^iBr^+$ ion signals. Relative ion signals depend, however, to some extent, on the laser power. One-dimensional (1D) REMPI spectra for individual ions are derived by integrating mass signals as a function of two-photon excitation wavenumber. Whereas relative intensities in different ion 1D REMPI depend on the laser power, the structure of the individual spectra is found to be largely independent of the ion. This can be seen in Figure 1b for the 66 022 cm^{-1} system. Figure 1c shows the $CH_3{}^+$ 1D REMPI spectrum for the wavenumber region 66 000−81 000 cm^{-1}. It agrees well with the recently published spectrum by Ridley et al.,[18] showing characteristic subspectra due to resonance transitions to Rydberg states, with gradually rising background as the energy increases, most probably due to an increasing contribution from transitions to the ion-pair state.[19]

Bands due to transitions to the zero vibrational energy levels of the [3/2]np;ω, [1/2]np;ω, [3/2]nd;ω, and [1/2]nd;ω Rydberg states from the zero vibrational energy level of the ground state, as assigned by Ridley et al.,[18] are identified and marked in Figure 1c with solid line bars above the $CH_3{}^+$ 1D REMPI spectrum. In addition,we have assigned bands due to transitions from the ground electronic and vibrational state to vibrationally excited levels of the [Ω_c]nl;0 states. These are listed in Table 1 and marked in Figure 1c with broken line bars for clear (Strong−Medium intensity) bands. Less intense (Weak−Very Weak) bands, only observable at enhanced laser power, are also listed in Table 1. Some of these bands correspond to vibronic bands observed in absorption spectra (albeit transition wavenumbers are offset by about 20− 30 cm^{-1} (see Table 1)) assigned by Causley and Russel.[2] These assignments as well as those given by Ridley et al.[18] disagree with those given by Locht et al.[5] Our assignment of the vibrational bands was guided by the following.

(i) Generally the strongest spectral features previously observed in absorption spectra[2,4,5] match the strongest features observed in our 1D (2+n) REMPI spectra. Since the potential energy surfaces for the Rydberg states closely resemble those for the ground states of CH_3Br and CH_3Br^+,[19] there is reason to believe that the strongest spectral features are due to transitions corresponding to unaltered vibrational energy, i.e., that $\Delta v_i = 0$ transitions are the most Franck−Condon-factor (FCF) favorable for all i. Furthermore, we expect transitions to become less FCF favorable as vibrational quantum numbers for the excited states deviate more from the original zero energy level; i.e., the transition strength (intensities) will change as ($v_i' = 0$) > ($v_i' = 1$) > ($v_i' = 2$), etc.

(ii) Frequencies of vibrational modes for Rydberg states are expected to be close to those in the ground states $CH_3Br(X)$ and $CH_3Br^+(X)$.[2,5] Hence, available experimental[37] and calculated[5,38] vibrational frequencies for $CH_3Br(X)$ and $CH_3Br^+(X)$ were useful in assigning vibrational bands. The v_i' notation used (Figure 1c, Table 1) assumes a_1 symmetry (valid for the ground state CH_3Br X^1A_1) to be a good approximation for the Rydberg states.[2] Alternatively a′ symmetry notations (valid for the ground state CH_3Br^+ X^2A') could be used, in which case $v_1(a_1)$ corresponds to $v_2(a')$, $v_2(a_1)$ to $v_4(a')$, and $v_3(a_1)$ to $v_6(a')$.[5] The vibrational assignment is further detailed in Table 1.

(iii) We expect a close analogy in the spectroscopy of the methyl halides (CH_3X; X = Cl, Br, I) and the corresponding hydrogen halides (HX).[18,19] Hence, the major Rydberg spectral features will be due to transitions from the ground state to nl_e Rydberg states (C_{3v} notation; nl_π states in $C_{\infty v}$ notation), i.e., due to transitions of electrons from lone pair e orbitals (C_{3v}

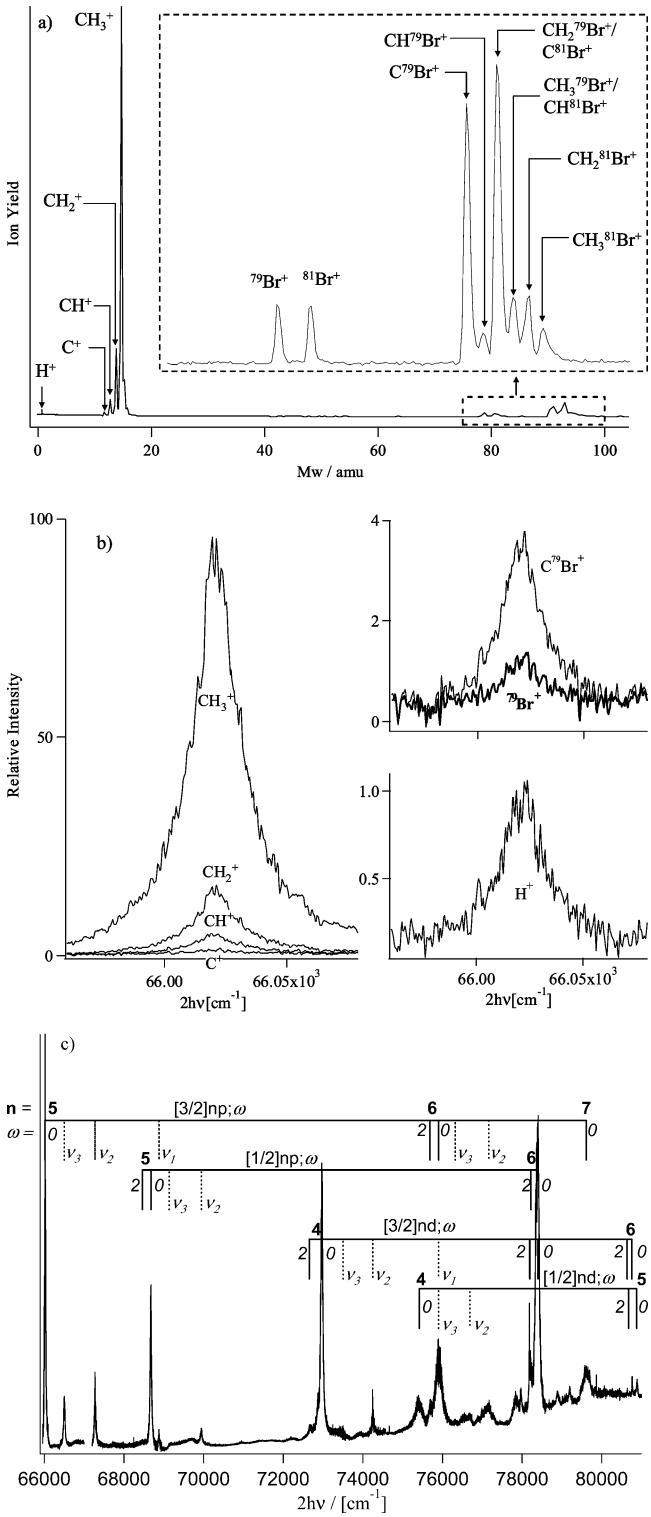

Figure 1. (a) Mass spectra for the two-photon excitation wavenumber 66 022 cm^{-1} corresponding to transition to the [3/2]5p;0,(0,0,0) Rydberg state (see Table 1); low resolution (below) and high resolution (above). (b) M^+ 1D REMPI spectra ($M^+ = CH_n^+$ ($n = 0-3$), $C^{79}Cr^+$, $^{79}Br^+$, and H^+) for two-photon transitions to the (3/2)5p;0,(0,0,0) Rydberg state (see Table 1). (c) CH_3^+ 1D REMPI spectrum and assignment of Rydberg states ($[\Omega_c]nl$; ω, (υ_1, υ_2, υ_3)) for the two-photon wavenumber region 66 000−81 000 cm^{-1}. Principal quantum numbers (n) of Rydberg states are marked in bold. Total angular momentum quantum numbers for Rydberg electrons (ω) are marked in italic. Vibrational quanta for vibrational modes ν_i; $i = 1, 2, 3$ (see text) of Rydberg states are marked as υ_1, υ_2, and υ_3; unlabeled peaks correspond to transitions to the zero vibrational energy levels, (υ_1, υ_2, υ_3) = (0, 0, 0), whereas peaks labeled υ_i are due to transitions to vibrational states $\upsilon_i = 1$ and $\upsilon_j = 0$ ($j \neq i$).

TABLE 1: Assignments and Transition Wavenumbers of Bands Due to Transitions from Ground State CH_3Br to Vibrationally Excited Rydberg States

assignment $[\Omega_c]nl$; ω, (υ_1, υ_2, υ_3)[a]	ν/cm^{-1} this work (intensity)[c]	ν/cm^{-1} ref 2
[3/2]*n*p:		
[3/2]5p;0,(0, 0,1)	66 503 (M)	66 482
[3/2]5p;0,(0, 1, 0)	67 275 (M)	67 246
[3/2]5p;0,(1, 0, 0)	68 882 (M)	68 848
[3/2]6p;0,(0, 0, 1)	76 323 (W)	
[3/2]6p;0,(0, 1, 0)	77 165 (M)	
[1/2]*n*p:		
[1/2]5p;0,(0, 0, 1)	69 137 (W)	69 105
[1/2]5p;0,(0, 1, 0)	69 947 (M)	69 932
[1/2]5p;0,(0, 2, 0)	70 948 (VW)	
[3/2]*n*d:		
[3/2]4d;0,(0, 0, 1)	73 507 (VW)	
[3/2]4d;0,(0, 1, 0)	74 249 (M)	
[3/2]4d;0,(1, 0, 0)	(75 905)[b]	
[3/2]5d;0,(0, 0, 1)	78 890 (M)	
[1/2]*n*d:		
[1/2]4d;0,(0, 0, 1)	(75 905)[b]	
[1/2]4d;0,(0, 1, 0)	76 689 (M)	
[1/2]4d;0,(0, 2, 0)	77 845 (M)	

[a] $[\Omega_c]$: total angular momentum quantum number for core ion. n: principal quantum number for Rydberg electron. l: Rydberg electron orbital (p, d). ω: total angular momentum quantum number for Rydberg electron. (υ_1, υ_2, υ_3): vibrational quantum numbers referring to vibrational modes. ν_1 (symmetric stretch), ν_2 (umbrella) and ν_3 (C−Br stretch).[5] [b] Spectral overlap [c] VW: very weak. W: weak. M: medium.

notation; π orbital in $C_{\infty v}$ notation) with dominant Br (for X = Br) character to high energy lone pair orbitals (l). Rydberg spectra due to transitions from bonding a_1 orbitals (C_{3v} notation; σ orbital in $C_{\infty v}$ notation) to high energy lone pair orbitals are not expected to play a major role.[18]

C Atom REMPI; C/C* Formation Channels. The very weak C^+ REMPI signal, following excitations to Rydberg states or the ion-pair state (see Figure 1a,b), largely shows the same spectral structure as the much stronger CH_3^+ REMPI signals (see Figures 1c and 2a) in the spectral region 66 000−80 600 cm^{-1} except for medium strong C atom REMPI lines, which appear in the excitation region 69 500−77 500 cm^{-1} (see Figure 2a). The C^+ 1D REMPI spectrum in the region 80 600−80 950 cm^{-1}, on the other hand, is far stronger, showing overall intensity comparable to the CH_3^+ REMPI. The structure, however, differs, to some extent, from that of the CH_3^+ 1D REMPI spectrum, as seen in Figure 2b. Observed C atom REMPI lines are listed in Table 2 along with predicted wavenumbers derived from known energy levels.[37] Relative line intensities are indicated. Lines due to resonance excitations of ground state C atoms (^3P_J; $J = 0$, 1, 2) and first excited state C*($^1D_2$) atoms are observed. Only spin conserved ($\Delta S = 0$) transitions are detected. All the observed C atom lines correspond to electron transfers of 2p electrons to np ($n > 2$) orbitals, which satisfy $\Delta l = 0$, $|\Delta L| \leq 2$, and $|\Delta J| \leq 2$, as expected for two-photon resonance transitions.

Energetically, the C atom REMPI signal can be explained by the formation of C and C* atoms by $CH_3Br^{**} \rightarrow H_2 + C + HBr$ ($E_0 \sim 58\,840$ cm^{-1} from the ground state CH_3Br)[39,40] and/or $CH_3Br^{**} \rightarrow H_2 + C^* + HBr$ ($E_0 \sim 69\,032$ cm^{-1}),[39,40] followed by (2+1)REMPI of C/C* (see Figure 3a),

$$CH_3Br + 2h\nu \rightarrow CH_3Br^{**}(Ry,i\text{-}p) \qquad (1a)$$

$$CH_3Br^{**}(Ry) \rightarrow H_2 + C/C^* + HBr \quad (1b)$$

$$C/C^* + 2h\nu \rightarrow C^{**} \quad (1c)$$

$$C^{**} + h\nu \rightarrow C^+ + e^- \quad (1d)$$

Formation of 2H + C/C* + HBr, H_2 + C/C* + H + Br, or 3H + Br + C/C* instead of (1b) is very unlikely on the basis of the bond energies of H_2 and HBr, 36 120 and 30 310 cm^{-1}, respectively.[39] These would necessitate that (1a) is replaced by a three- or four-photon processes, which puts the intermediate already in the ionization continuum. It is unlikely that such a highly energetic intermediate species does not autoionize and that consecutive H, Br, H_2, or HBr losses accompanied by significant kinetic energy release leave it with enough internal energy to form C atoms. An alternative H_2 + C/C* + HBr formation via initial excitation of dimers cannot be fully ruled out. Since we operated the jet in conditions that limited cooling (see Experimental Section) and no ion signals for dimers were observed, we feel, however, that its involvement is not of major importance. Even in the unlikely case that initial dimer excitation contributes to the observed fragmentation channel, it is very unlikely that this opens up new reaction channels, and the nonfragmenting CH_3Br could, thus, only act as a spectator, possibly enhancing fragmentation, but not affecting the energetics of the process. The (1a)−(1d) mechanism gains further support from (i) the observation of HBr REMPI signals, (ii) the enhanced C^+ REMPI signal above 80 600 cm^{-1}, (iii) relative intensities of C atom REMPI signals, (iv) power dependence data, and (v) potential energy surface (PES) calculations. These will now be discussed.

(i) The C atom REMPI lines at 75 204.6 cm^{-1} (C**(5p, $^1D_2$) ←← C*(2p^2, $^1D_2$)) and 75 429.6 cm^{-1} (C**(5p, $^1S_0$) ←← C*(2p^2, $^1D_2$)) follow excitations to the [1/2]4d;0,(0,0,0) Rydberg state whereas the C atom REMPI lines at 77 023.3 cm^{-1} (C**(6p,

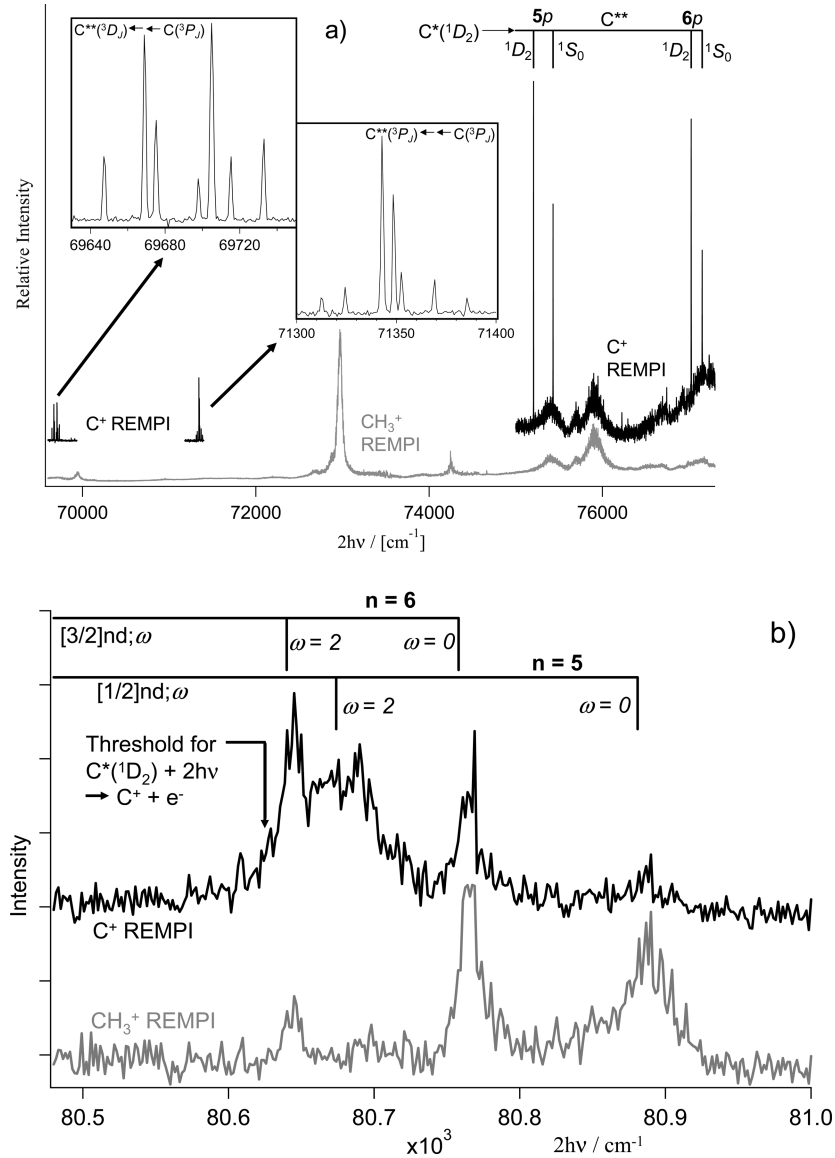

Figure 2. C^+ REMPI. (a) C^+ 1D REMPI spectra (bold) along with the CH_3^+ 1D REMPI spectrum (Figure 1c) (gray) for the two-photon wavenumber region 69 500−77 500 cm^{-1}. Insets show the spectral regions 69 640−69 740 and 71 300−71 400 cm^{-1}. Peaks due to two-photon resonance transitions from C(^3P_J) (insets) and from C*($^1D_2$) (top right) to C atom Rydberg states (C**) are labeled. See also Table 2. (b) C^+ 1D REMPI spectra (bold; above) along with the CH_3^+ 1D REMPI spectrum (Figure 1c) (gray; below) for the two-photon wavenumber region 80 500−81 000 cm^{-1}. Assignment of Rydberg states ($[\Omega_c]nl;\omega$, (v_1, v_2, v_3)) is shown (see caption for Figure 1c for further clarification). The energy threshold for two-photon ionization of C*($^1D_2$) (80 625.27 cm^{-1}) is also shown.

TABLE 2: Carbon Atomic Lines (cm^{-1}) Due to (2+1) REMPI of $C(2s^22p^2;^3P_J)$ (a) and $C^*(2s^22p^2;^1D_2)$ (b), Following Two-Photon Excitation of CH_3Br vs Carbon Excited States (C) (and Term Symbols) and Predicted Wavenumber Values Derived from Energy Levels[37] (Line Strengths Indicated)[a]**

Table (a)

	$C(2s^22p^2;\ ^3P_0)$		$C(2s^22p^2;\ ^3P_1)$		$C(2s^22p^2;\ ^3P_2)$	
terms/$^{2S'+1}X_{J'}$ $(2s^22p(^2P)3p)$	this work (intensity[a])	NIST[b]	this work (intensity[a])	NIST[b]	this work (intensity[a])	NIST[b]
$^3D_1$	*c*	69 689.48	69 675.3 (W)	69 673.08	69 647.2 (W)	69 646.08
$^3D_2$	69 715.4 (W)	69 710.66	69 697.7 (W)	69 694.26	69 668.9 (M)	69 667.26
$^3D_3$	*c*	69 744.03	69 733.1 (W)	69 727.63	69 705.0 (M)	69 700.63
$^3P_0$	71 352.9 (W)	71 352.51	*c*	71 336.11	71 312.3 (VW)	71 309.11
$^3P_1$	*c*	71 364.90	71 348.9 (W)	71 348.50	71 324.3 (VW)	71 321.50
$^3P_2$	71 385.4 (VW)	71 385.38	71 369.1 (VW)	71 368.98	71 343.0 (W)	71 341.98

Table (b)

		$C(2s^22p^2;\ ^1D_2)$	
configuration; excited states	terms/$^{2S'+1}X_{J'}$	this work (intensity[a])	NIST[b]
$2s^22p(^2P)4p$	$^1D_2$	71 577.0 (VW)	71 577.16
$2s^22p(^2P)4p$	$^1S_0$	72 062.0 (VW)	72 059.08
$2s^22p(^2P)5p$	$^1D_2$	75 204.6 (M)	75 207.18
$2s^22p(^2P)5p$	$^1S_0$	75 429.6 (M)	75 432.55
$2s^22p(^2P)6p$	$^1D_2$	77 023.3 (M)	77 025.63
$2s^22p(^2P)6p$	$^1S_0$	77 150.8 (M)	77 148.41

[a] M: medium. W: weak. VW: very weak. [b] Reference 37. [c] Not observed.

$^1D_2$) ←— $C^*(2p^2,\ ^1D_2)$) and 77 150.8 cm^{-1} ($C^{**}(6p,\ ^1S_0)$ ←— $C^*(2p^2,\ ^1D_2)$) follow transitions to the [3/2]6p;0,(0,1,0) state (see Figures 1c and 2a and Tables 1 and 2b). Weak HBr REMPI signals, due to the two-photon resonance transitions $g^3\Sigma^-$ ←— $X^1\Sigma^+(0,0)$ and $F^1\Delta_2$ ←— $X^1\Sigma^+(0,0)$,[32] are also found to appear near these atom resonances, following excitation to the same Rydberg states as seen in Figure 4. Since these observations are made under collision free conditions in a molecular beam, formation of HBr (and H_2) by secondary radical reactions can be ruled out. Therefore, these spectra are due to (2+1)REMPI of $HBr(X^1\Sigma^+;v''=0,J'')$ most probably following steps (1a) and (1b) for the corresponding CH_3Br Rydberg states and $C^*(2p^2,\ ^1D_2)$ atom formation,

$$CH_3Br + 2h\nu \rightarrow CH_3Br^{**}(4d/6p,i\text{-}p) \qquad (2a)$$

$$CH_3Br^{**}(4d/6p) \rightarrow H_2 + C^*(2p^2,{}^1D_2) + HBr(X) \qquad (2b)$$

$$HBr(X) + 2h\nu \rightarrow HBr^{**}(g^3\Sigma^-,\nu' = 0,J')/\ HBr^{**}(F^1\Delta_2,\nu' = 0,J') \qquad (2c)$$

$$HBr^{**} + h\nu \rightarrow HBr^+ + e^- \qquad (2d)$$

In addition to the rotational lines ($J = J' = J'' = 0 - 8$; Q line) observed by Gallagher and Gordon[32] for the HBr, $g^3\Sigma^-$ ←— $X^1\Sigma^+(0,0)$ system, lines for $J > 8$ also are observed. This, as well as preliminary simulation calculations of the HBr (2+1)REMPI spectrum, suggests that $HBr(X^1\Sigma^+;v'' = 0,J'')$ molecules formed by (2b) are rotationally hot.

(ii) The observed intensity enhancement in the C^+ REMPI signal in the region above 80 600 cm^{-1} (see Figure 2b) can be explained as being due to switching from three-photon to two-photon ionization of $C^*(^1D_2)$ formed by step (2b), the threshold for which is the ionization potential for $C^*(^1D_2)$ (80 625.27 cm^{-1}).[37] This strongly suggests that not only the C atom REMPI signal but also the "nonresonant" REMPI C^+ signal are due to photoionization of C/C* atoms after their formation by photodissociation in this spectral region. Generally, the CH_3^+ REMPI signal for excitation to $\omega = 2$ states is much weaker than the corresponding signal for $\omega = 0$ states (see Figures 1c and 2b). The opposite is found for the C^+ REMPI signals in the region 80 600−81 000 cm^{-1}. Although the formation mechanism for CH_3^+, hence the CH_3^+ REMPI signal's origin, is not certain, this indicates that dissociation of $\omega = 2$ states, to form H_2 + $C^*(^1D_2)$ + HBr, is favored over that of dissociation of $\omega = 0$ states.

(iii) Whereas the C atom REMPI signal due to two-photon resonance excitations of $C^*(^1D_2)$ to the 5p and 6p states are medium strong (see Figure 2a and Table 2b), transitions to the 4p states are very weak (not shown in Figure 2a). Since there is reason to believe that the transition probabilities for the lower energy transitions to the 4p states are in fact larger than those to the 5p and 6p states, this observation suggests that there is a barrier on the potential energy surface for the transformations of $CH_3Br^{**}(Ry)$ to H_2 + $C^*(^1D_2)$ + HBr (E = 69 522 cm^{-1}) by step (1b) close to that of the excitation energies needed for the $C^{**}(4p,\ ^1D_2/^1S_0)$ ←— $C^*(^1D_2)$ transitions (71 577−72 062 cm^{-1}), i.e., in the vicinity of 72 000 cm^{-1}.

(iv) Slope values slightly larger than 3 were derived from log−log plots for C atom REMPI signals vs laser power for the medium strong atom lines at 69 668.9 cm^{-1} ($C^{**}(3p,^3D_2)$ ←— $C(2p^2,\ ^3P_2)$) and 69 705.0 cm^{-1} ($C^{**}(3p,^3D_2)$ ←— $C(2p^2,\ ^3P_2)$), respectively. A slope value of 5 is to be expected in the low laser power limit for the overall ($2_r + 2_r' + 1_i$) REMPI process, where 2_r and $2_r'$ refer to the two-photon resonance steps (1a) and (1c), respectively, and 1_i refers to the one-photon ionization step (1d). A slope value higher than 5 could indicate a three-photon initial step, instead of (2a), and rule out the proposed mechanism. The observed slope value, slightly higher than 3, could indicate a near saturation effect in the Rydberg excitation step (1a), difficult to avoid when looking for the relatively weak atom signals. In fact, saturation of step (1a) may be necessary for the presumably very low quantum efficiency step (1b) to proceed to a measurable degree.

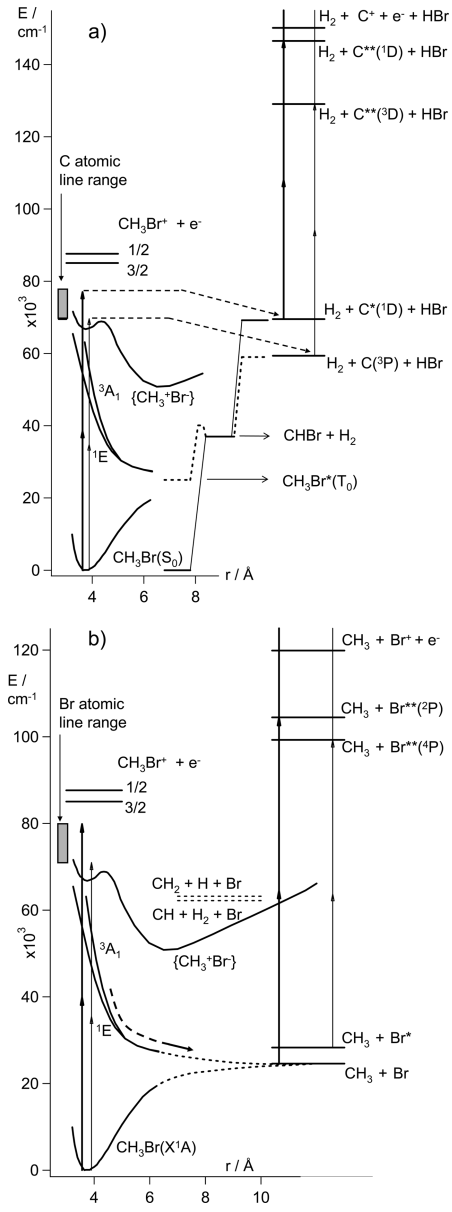

Figure 3. Schematic energy diagrams relevant to C^+ (a) and Br^+ (b) REMPI data, showing calculated potential energies as functions of the CH_3-Br bond distance[13,19] as well as relevant energy thresholds and transitions. (a) Transitions involving (2_r+1_i) REMPI (see text) of $C^*(^1D_2)$ (77 023.3 cm^{-1}; $C^{**}(6p,^1D_2) \leftarrow\!\!-\!\!- C^*$) and $C(^3P_2)$ (69 668.9 cm^{-1}; $C^{**}(3p,^3D_2) \leftarrow\!\!-\!\!- C$) following two-photon excitations of CH_3Br to the Rydberg/ion-pair manifold and photodissociation to form H_2 + C/C* + HBr (broken arrows) are shown as bold and narrow line arrows, respectively. Calculated thresholds (see text) for transformation of methyl bromide in the lowest energy singlet state (CH_3Br (S_0)), via CHBr + H_2 formation, to $H_2 + C^*(^1D)$ + HBr are shown as solid line energy levels joined by unbroken lines. Calculated thresholds and the energy barrier (see text) for transformation of methyl bromide in the lowest energy triplet state (CH_3Br (T_0)), via CHBr + H_2 formation, to $H_2 + C\ (^3P)$ + HBr are shown as broken line energy levels joined by broken lines. The excitation region for carbon atomic line detection is also indicated. (b) Transitions involving (2_r+1_i) REMPI (see text) of $Br(^2P_{3/2})$ (79 866.8 cm^{-1}; $Br^{**}(^2P_{1/2}) \leftarrow\!\!-\!\!- Br$) and $Br^*(^2P_{1/2})$ (70 987.5 cm^{-1}; $Br^{**}(^4P_{5/2}) \leftarrow\!\!-\!\!- Br^*$) following two-photon excitations of CH_3Br to the Rydberg/ion-pair manifold and photodissociation to form CH_3 + Br/Br* are shown as bold and narrow line arrows, respectively. The excitation region for bromine atomic line detection is also indicated.

(v) For the proposed mechanism (1a)−(1d) to be feasible, the overall barrier to the $CH_3Br \rightarrow H_2$ + C/C* + HBr reaction has to be smaller than the initial two-photon excitation energy

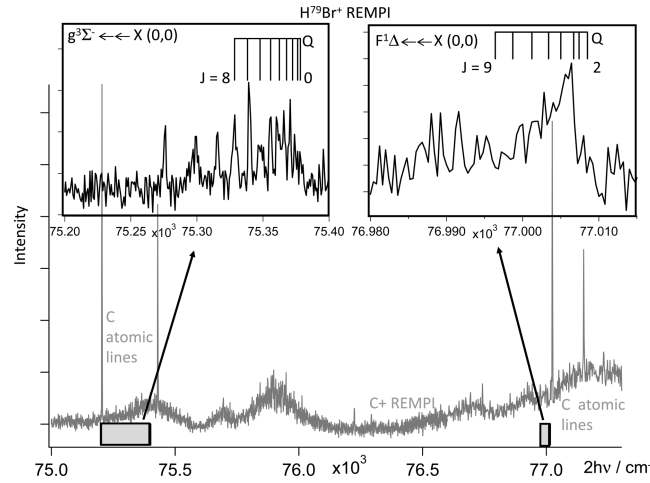

Figure 4. HBr^+ 1D (2_r+1_i) REMPI spectra (top insets) along with the C^+ 1D REMPI spectrum (Figure 4a) (gray). The HBr^+ spectrum for the spectral region 75 200−75 400 cm^{-1} (top, left) shows rotational structure due to the two-photon resonance transition $g^3\Sigma^- \leftarrow\!\!-\!\!- X^1\Sigma^+$ (0,0).[32] The HBr^+ spectrum for the spectral region 76 980−77 015 cm^{-1} (top, right) shows rotational contour due to the two-photon resonance transition $F^1D_2 \leftarrow\!\!-\!\!- X^1\Sigma^+$ (0,0).[32] Rotational line positions for HBr, determined by Callaghan and Gordon,[32] are shown.

for CH_3Br in step (1a). By analogy to our analysis for photodissociation of acetylene (C_2H_2) to form $C_2 + H_2$,[35] we searched for the lowest energy thresholds for this dissociation by calculating potential energy surfaces (PES) for transformations of the lowest energy singlet and triplet states of methyl bromide (CH_3Br (S_0) and CH_3Br (T_0)) to $H_2 + C^*(^1D_2)$ + HBr and H_2 + $C(^3P)$ + HBr, respectively. The potential energy surfaces for the singlet and triplet states were calculated with Gaussian03[41] at the B3LYP/6-311++G(d,p) level of theory. First, simultaneous H_2 and HBr loss was studied by carrying out a 2D potential energy surface scan, in which an H_2 and a HBr molecule were allowed to approach the carbon core in constrained geometry optimizations. The simultaneous H_2 + HBr loss appears to be monotonously uphill in energy and, therefore, not particularly likely. Second, when HBr was allowed to approach C by constraining the C−Br bond length, the H atom in HBr jumped over to C at a large distance. The time inverse process of a Br atom leaving the core and the H following it with a ca. 3 Å delay is extremely unlikely. Therefore, it is suggested that (1b) takes place in two steps, the first being the ejection of an H_2 molecule. This process is found to take place without a reverse barrier on the ground singlet surface. The second step, the loss of HBr from HCBr is energetically very similar to Br atom loss and takes place practically without a reverse barrier on the ground singlet and triplet surfaces. Thus, we conclude that the proposed mechanism (1a)−(1d) is energetically feasible, as shown schematically in Figure 3a.

Br Atom REMPI; Br/Br* Formation Channels. The weak Br^+ REMPI signals, following excitations to Rydberg states or the ion-pair state (see Figure 1a,b), show the same overall spectral structure as the stronger CH_3^+ REMPI signals (Figure 1c) except for strong Br atom REMPI lines that appear in the excitation region 70 950−79 900 cm^{-1} (see Figure 5). Lines due to resonance excitations of both ground state spin−orbit components, $Br(^2P_{3/2})$ and $Br^*(^2P_{1/2})$, are observed. Both spin conserved ($\Delta S = 0$) and spin-flip ($\Delta S = 2$) transitions are identified. All observed Br atom lines correspond to electron transfers of 4p electrons to 5p orbitals, which satisfy $\Delta l = 0$, $|\Delta L| \leq 2$, and $|\Delta J| \leq 2$ as to be expected for two-photon

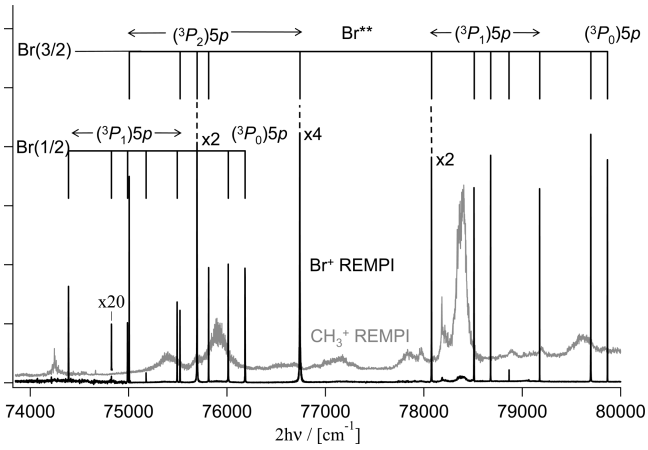

Figure 5. Br^+ 1D REMPI spectra (bold) along with the CH_3^+ 1D REMPI spectrum (Figure 1c) (gray) for the two-photon wavenumber region 74 000−80 000 cm^{-1}. Peaks due to two-photon resonance transitions from $Br(4p^5;^2P_{3/2})$ (top) and $Br(4p^5;^2P_{1/2})$ (below) to $Br^{**}((^3P_J)_c;5p)$, where $(^3P_J)_c$ is the ion core term, are labeled. The strongest atomic lines at 75 696.4 cm^{-1} ($^4D_{5/2} \leftarrow\!\!\leftarrow {}^2P_{3/2}$), 76 742.4 cm^{-1} ($^4D_{3/2} \leftarrow\!\!\leftarrow {}^2P_{3/2}$), and 78 079.6 cm^{-1} ($^2S_{1/2} \leftarrow\!\!\leftarrow {}^2P_{3/2}$) have been scaled down by factors 2, 4, and 2, respectively, as indicated.

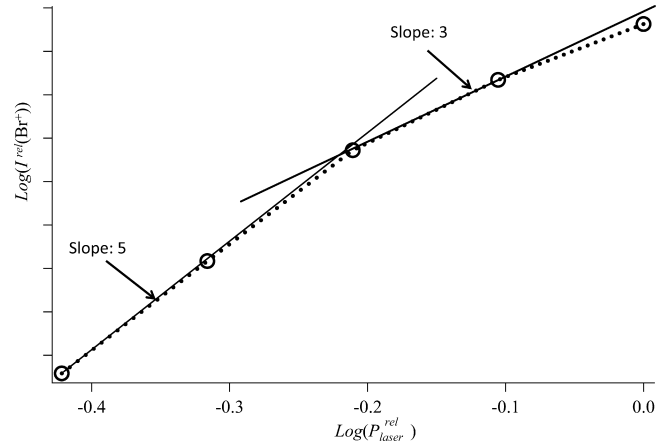

Figure 6. Power dependence of the $^{79}Br^+$ ion signal at 78 680.0 cm^{-1} due to the two-photon bromine atomic resonance transition $^2D_{3/2} \leftarrow\!\!\leftarrow {}^2P_{3/2}$. Log−log plot of the relative $^{79}Br^+$ ion intensity ($I^{rel}(^{79}Br^+)$) as a function of relative laser power (P^{rel}_{laser}), i.e., $\log(I^{rel}(^{79}Br^+))$ vs $\log(P^{rel}_{laser})$ (circles joined by straight lines). Lines for slopes 5 and 3 are inserted.

resonance transitions.[37,42] In addition to the lines shown in Figure 5, very weak lines are observed at 70 987.5 and 70 987.08 cm^{-1} due to the $^4P_{5/2} \leftarrow\!\!\leftarrow {}^2P_{1/2}$ and $^4P_{3/2} \leftarrow\!\!\leftarrow {}^2P_{1/2}$ transitions, respectively.[37]

The Br atom REMPI signal may be due to resonance excitations of Br and Br* atoms formed by predissociation of excited Rydberg states after two-photon excitation of CH_3Br to Rydberg states or the ion-pair state (CH_3Br^{**}(Ry,i-p)) (see Figure 3b), i.e.

$$CH_3Br + 2h\nu \rightarrow CH_3Br^{**}(Ry,i\text{-}p) \quad (3a)$$

$$CH_3Br^{**}(Ry) \rightarrow CH_3 + Br/Br^* \quad (3b)$$

$$Br/Br^* + 2h\nu \rightarrow Br^{**} \quad (3c)$$

$$Br^{**} + h\nu \rightarrow Br^+ + e^- \quad (3d)$$

The ion-pair state is known to couple strongly to Rydberg states of the same symmetry,[43] and by analogy to the hydrogen halides (HX), coupling beyond symmetry restrictions could also occur. Couplings between singlet and triplet Δ-Rydberg states (Ω = 2, 1) as well as a $^3\Sigma^+(\Omega{=}1)$ Rydberg state and the ion-pair state $V\ ^1\Sigma^+(\Omega{=}0)$ have been observed in HCl.[25−27,34,36] Predissociation, which occurs by crossing from Rydberg states to repulsive valence states may involve a gateway Rydberg state (i.e., a Rydberg−Rydberg interaction) by analogy to the hydrogen halide systems.[25,44] Alternatively, Br and Br* atoms may be formed by dissociation of CH_3Br^{**} to form CH + H_2 + Br/Br* and/or CH_2 + H + Br/Br* fragments instead of channel (1b) (see Figure 3b).

The above mechanism (3a)−(3d) further gains support from power dependence experimental data. Figure 6 shows the log−log plot for the ^{79}Br atom REMPI signal of the strong 78 680.0 cm^{-1} atom line ($^2D_{3/2} \leftarrow\!\!\leftarrow {}^2P_{3/2}$ transition) as a function of laser power. The observed curvature of the plot, as laser power increases, indicates a saturation effect.[45] Slope evaluations reveal the number of photons needed to create $^{79}Br^+$ ions for low laser power to be 5. This value fits the total number of photons in the overall ($2_r + 2_r' + 1_i$) REMPI process. A slope value derived for higher power (ca. 3; see Figure 6) could be due to saturation in the CH_3Br^{**}(Ry,i-p) formation step (3a), in which case the ion signal will increase proportionally to the laser power cubed ($2_r' + 1_i$). Further "leveling off" in the log−log plot as power increases could indicate additional saturation in the Br atom resonance step (3c). A slope value close to 5 was also derived in the low laser power limit for the ^{79}Br atom REMPI signal at 74 389.6 cm^{-1} ($^2S_{1/2} \leftarrow\!\!\leftarrow {}^2P_{1/2}$ transition).

Conclusions

2D REMPI spectra for CH_3Br were recorded for the two-photon resonance excitation region 66 000−81 000 cm^{-1} by recording ion TOF spectra as a function of the laser frequency. Most spectral features could be assigned on the basis of previous absorption[2,4,5] and REMPI[18] spectra as well as ab initio calculations.[5,19] These, however, disagree with assignments given by Locht et al.[5] The major spectral structure is due to two-photon electron transitions of lone pair electrons to *n*p and *n*d orbitals localized on the Br atom to produce Rydberg states converging to either of the two (Ω_c = 3/2, 1/2) spin−orbit states of the molecular ion for total electronic angular momentum quantum numbers (ω) 0 or 2. In addition to previously assigned bands in REMPI due to transitions involving no vibrational excitation, i.e., 0−0 transitions,[18] transitions involving one or two quanta in a single vibrational mode only ($\Delta\nu_i = 1, 2$; $\Delta\nu_j = 0, j \neq i$) were also observed. An observed rise in background REMPI signal with increasing energy is attributed to a gradually increasing contribution from transitions to the ion-pair state, as was previously predicted.[19]

Medium strong carbon (2+1) REMPI signals are observed in the 69 500−77 500 cm^{-1} region due to transitions from ground triplet state $C(^3P)$ atoms and the first excited singlet state $C^*(^1D_2)$ atoms. Most probably, these are due to resonance excitations after dissociation of CH_3Br^{**} Rydberg states, initially created by two-photon excitation, to form H_2 + C/C* + HBr fragments. HBr REMPI signals, enhanced intensities of C^+ REMPI signals above 80 600 cm^{-1}, power dependence data, energy considerations, and potential energy surface calculations support this mechanism. An increased relative intensity of the C atom 5p and 6p REMPI signal compared with the 4p signal

suggests that there is a barrier along the photodissociation pathway. To our knowledge this is the first indication of a photodissociative channel in a small molecule, in which four bonds are broken and two bonds are formed.

The strong bromine (2+1) REMPI signals in the 70 950−79 900 cm^{-1} region and its power dependence behavior suggest that $Br(^2P_{3/2})$ and $Br^*(^2P_{1/2})$ atoms are formed by predissociation of Rydberg states after initial two-photon excitation. Predissociation to form CH_3 + Br/Br* may give rise to this signal.

Acknowledgment. The financial support of the University Research Fund, University of Iceland, and the Icelandic Science Foundation is gratefully acknowledged. We thank Helgi Rafn Hródmarsson for useful help with the project.

References and Notes

(1) Price, W. C. *J. Chem. Phys.* **1936**, *4*, 539.
(2) Causley, G. C.; Russell, B. R. *J. Chem. Phys.* **1975**, *62*, 848.
(3) Felps, S.; Hochmann, P.; Brint, P.; McGlynn, S. P. *J. Mol. Spectrosc.* **1976**, *59*, 355.
(4) Locht, R.; Leyh, B.; Jochims, H. W.; Baumgartel, H. *Chem. Phys.* **2005**, *317*, 73.
(5) Locht, R.; Leyh, B.; Dehareng, D.; Jochims, H. W.; Baumgartel, H. *Chem. Phys.* **2005**, *317*, 87.
(6) Molina, L. T.; Molina, M. J.; Rowland, F. S. *J. Phys. Chem.* **1982**, *86*, 2672.
(7) Vanveen, G. N. A.; Baller, T.; Devries, A. E. *Chem. Phys.* **1985**, *92*, 59.
(8) Hess, W. P.; Chandler, D. W.; Thoman, J. W. *Chem. Phys.* **1992**, *163*, 277.
(9) Gougousi, T.; Samartzis, P. C.; Kitsopoulos, T. N. *J. Chem. Phys.* **1998**, *108*, 5742.
(10) Blanchet, V.; Samartzis, P. C.; Wodtke, A. M. *J. Chem. Phys.* **2009**, *130*.
(11) Shaw, D. A.; Holland, D. M. P.; Walker, I. C. *J. Phys. B-At. Mol. Opt. Phys.* **2006**, *39*, 3549.
(12) Xu, D. D.; Huang, J. H.; Price, R. J.; Jackson, W. M. *J. Phys. Chem. A* **2004**, *108*, 9916.
(13) Escure, C.; Leininger, T.; Lepetit, B. *J. Chem. Phys.* **2009**, *130*, 244305.
(14) Robbins, D. E. *Geophys. Res. Lett.* **1976**, *3*, 213.
(15) Robbins, D. E. *Geophys. Res. Lett.* **1976**, *3*, 757.
(16) Warwick, N. J.; Pyle, J. A.; Shallcross, D. E. *J. Atmos. Chem.* **2006**, *54*, 133.
(17) http://cienbas.galeon.com/04GW_Potential.htm; US Environmental Protection Agency Class I Ozone-Depleting Substances.
(18) Ridley, T.; Hennessy, J. T.; Donovan, R. J.; Lawley, K. P.; Wang, S.; Brint, P.; Lane, E. *J. Phys. Chem. A* **2008**, *112*, 7170.
(19) Escure, C.; Leininger, T.; Lepetit, B. *J. Chem. Phys.* **2009**, *130*, 244306.
(20) Yencha, A. J.; Kela, D. K.; Donovan, R. J.; Hopkirk, A.; Kvaran, Á. *Chem. Phys. Lett.* **1990**, *165*, 283.
(21) Kvaran, Á.; Yencha, A. J.; K.Kela, D.; Donovan, R. J.; Hopkirk, A. *Chem. Phys. Lett.* **1991**, *179*, 263.
(22) Kaur, D.; Yencha, A. J.; Donovan, R. J.; Kvaran, Á.; Hopkirk, A. *Org. Mass Spectrom.* **1993**, *28*, 327.
(23) Yencha, A. J.; Kaur, D.; Donovan, R. J.; Kvaran, Á.; Hopkirk, A.; Lefebvre-Brion, H.; Keller, F. *J. Chem. Phys.* **1993**, *99*, 4986.
(24) Lawley, K. P.; Flexen, A. C.; Maier, R. R. J.; Manck, A.; Ridley, T.; Donovan, R. J. *Phys. Chem. Chem. Phys.* **2002**, *4*, 1412.
(25) Kvaran, A.; Matthiasson, K.; Wang, H. *J. Chem. Phys.* **2009**, *131*, 044324.
(26) Kvaran, Á.; Wang, H. *J. Mol. Spectrosc.* **2004**, *228*, 143.
(27) Kvaran, Á.; Wang, H.; Logadóttir, Á. *J. Chem. Phys.* **2000**, *112*, 10811.
(28) Green, D. S.; Bickel, G. A.; Wallace, S. C. *J. Mol. Spectrosc.* **1991**, *150*, 303.
(29) Green, D. S.; Bickel, G. A.; Wallace, S. C. *J. Mol. Spectrosc.* **1991**, *150*, 354.
(30) Green, D. S.; Bickel, G. A.; Wallace, S. C. *J. Mol. Spectrosc.* **1991**, *150*, 388.
(31) Kvaran, Á.; Logadóttir, Á.; Wang, H. *J. Chem. Phys.* **1998**, *109*, 5856.
(32) Callaghan, R.; Gordon, R. J. *J. Chem. Phys.* **1990**, *93*, 4624.
(33) Wright, S. A.; McDonald, J. D. *J. Chem. Phys.* **1994**, *101*, 238.
(34) Kvaran, Á.; Matthíasson, K.; Wang, H.; Bodi, A.; Jonsson, E. *J. Chem. Phys.* **2008**, *129*, 164313.
(35) Matthiasson, K.; Wang, H. S.; Kvaran, A. *Chem. Phys. Lett.* **2008**, *458*, 58.
(36) Matthiasson, K.; Wang, H. S.; Kvaran, A. *J. Mol. Spectrosc.* **2009**, *255*, 1.
(37) NIST Chemistry WebBook; NIST (National Institute of Standards and Technology) Chemistry WebBook.
(38) Lugez, C. L.; Forney, D.; Jacox, M. E.; Irikura, K. K. *J. Chem. Phys.* **1997**, *106*, 489.
(39) Chase, M. W. *J.* **1998**, *4*, 1.
(40) Song, Y.; Qian, X. M.; Lau, K. C.; Ng, C. Y.; Liu, J. B.; Chen, W. W. *J. Chem. Phys.* **2001**, *115*, 4095.
(41) Frisch, M. J.; Trucks, G. W.; Schlegel, H. B.; Scuseria, G. E.; Robb, M. A.; Cheeseman, J. R.; Montgomery, J. A., Jr.; Vreven, T.; Kudin, K. N.; Burant, J. C.; Millam, J. M.; Iyengar, S. S.; Tomasi, J.; Barone, V.; Mennucci, B.; Cossi, M.; Scalmani, G.; Rega, N.; Petersson, G. A.; Nakatsuji, H.; Hada, M.; Ehara, M.; Toyota, K.; Fukuda, R.; Hasegawa, J.; Ishida, M.; Nakajima, T.; Honda, Y.; Kitao, O.; Nakai, H.; Klene, M.; Li, X.; Knox, J. E.; Hratchian, H. P.; Cross, J. B.; Bakken, V.; Adamo, C.; Jaramillo, J.; Gomperts, R.; Stratmann, R. E.; Yazyev, O.; Austin, A. J.; Cammi, R.; Pomelli, C.; Ochterski, J. W.; Ayala, P. Y.; Morokuma, K.; Voth, G. A.; Salvador, P.; Dannenberg, J. J.; Zakrzewski, V. G.; Dapprich, S.; Daniels, A. D.; Strain, M. C.; Farkas, O.; Malick, D. K.; Rabuck, A. D.; Raghavachari, K.; Foresman, J. B.; Ortiz, J. V.; Cui, Q.; Baboul, A. G.; Clifford, S.; Cioslowski, J.; Stefanov, B. B.; Liu, G.; Liashenko, A.; Piskorz, P.; Komaromi, I.; Martin, R. L.; Fox, D. J.; Keith, T.; Al-Laham, M. A.; Peng, C. Y.; Nanayakkara, A.; Challacombe, M.; Gill, P. M. W.; Johnson, B.; Chen, W.; Wong, M. W.; Gonzalez, C.; Pople, J. A. *Gaussian 03*, Revision C.02: Gaussian, Inc.: Pittsburgh, PA, 2004.
(42) Ridley, T.; Lawley, K. P.; Donovan, R. J.; Yencha, A. *J. Chem. Phys.* **1990**, *148*, 315.
(43) Escure, C.; Leininger, T.; Lepetit, B. *J. Chem. Phys.* **2009**, *130*.
(44) Alexander, M. H.; Li, X. N.; Liyanage, R.; Gordon, R. J. *Chem. Phys.* **1998**, *231*, 331.
(45) Sausa, R. C.; Pastel, R. L. "(2+2) Resonance Enhanced Multiphoton Ionization (REMPI) and Photoacoustic (PA) Spectroscopic Detection of Nitric Oxide (NO) and Nitrogen Dioxide (NO2) Near 454 nm," Army Research Laboratory, 1997.

JP104128J